

# **Domain structures of ferroelectric nanotubes controlled by surface charge compensation**

Jie Wang<sup>\*</sup> and Marc Kamlah  
Forschungszentrum Karlsruhe, Institute for Materials Research II  
Postfach 3640, 76021 Karlsruhe, Germany

## **Abstract**

Domain structures in ferroelectric nanotubes (FNTs) under different electrical boundary conditions are predicted through a phase field model. Simulation results show that domain structures are highly dependent on the compensation of polarization-induced surface charges. In order to reduce the depolarization energy, polarizations in FNTs form a vortex structure under an open-circuit boundary condition. When surface charges are compensated on the inner and outer surfaces, a multi-domain structure is formed in FNTs as a result of competition between the long-range electrostatic and elastic interactions. However, a single-domain structure is energetically favourable in FNTs if the upper and lower surfaces are short-circuited.

---

<sup>\*</sup> Corresponding author. Tel: +49 7247 82 5857, Fax: +49 7247 82 2347.  
E-mail address: jie.wang@imf.fzk.de

Nanoscale ferroelectric materials have received considerable attention from the academia and the industry due to the potential integration of nanoferroelectrics into microelectronics. The properties of ferroelectric materials in nanometer scale are substantially different from those of their bulk counterparts.<sup>1-3</sup> There are numerous theoretical and experimental investigations on ferroelectric nanostructures. However, most of the investigations focus on ferroelectric dots<sup>4,5</sup>, wires<sup>6,7</sup> and thin films.<sup>8,9</sup> Ferroelectric nanotubes (FNTs), which have a variety of potential applications that can not be filled by other nanotubes,<sup>10</sup> have not received much attention. Recently, individual FNTs and ferroelectric nanotube arrays have been successfully fabricated by different deposition techniques.<sup>11-13</sup> This opens opportunities to use FNTs in the fields such as photonics devices, MEMS devices, and data storage devices.

The physical properties of FNTs, such as the piezoelectric and photonic properties, are highly dependent on the polarization distribution or domain structures. However, the equilibrium domain structures in FNTs are still not well-understood due to their complex geometry, which increases difficulties in the experimental characterization and theoretical prediction of domain structures. The complex geometry may also generate a toroidal order in ferroelectric crystals in nanoscale.<sup>14</sup> On the other hand, different electrodes are needed for FNTs in different applications. Different electrodes provide different electrical boundary conditions for FNTs. Electrical boundary conditions can be used to control surface charge compensation in the formation of polarizations of FNTs. The charge compensation on the surfaces will affect equilibrium domain structures and thus change the physical properties of FNTs. Therefore, the prediction of equilibrium domain structures in FNTs is not only important in physics but also technically useful.

In this letter, we predict the equilibrium polarization distribution in FNTs with different electrical boundary conditions using a phase field model. The phase field model is based on the time-dependent Ginzburg-Landau equation, mechanical equilibrium equation and Gauss' law. It provides a powerful method to predict the polarization distribution in ferroelectric materials without any priori assumption. Similar phase field models have been employed to predict the equilibrium polarization distribution in ferroelectric nanodots<sup>15</sup> and thin films.<sup>16</sup> In the present phase field model, the total free energy of the ferroelectric system is obtained by integrating an electrical enthalpy over the whole volume. The electrical enthalpy is a function of polarization  $P_i$ , strain  $\varepsilon_{ij}$  and electric field  $E_i$ , which can be expressed as

$$h(P_i, \varepsilon_{ij}, E_i) = \alpha_i P_i^2 + \alpha_{ij} P_i^2 P_j^2 + \alpha_{ijk} P_i^2 P_j^2 P_k^2 + \frac{1}{2} c_{ijkl} \varepsilon_{ij} \varepsilon_{kl} - q_{ijkl} \varepsilon_{ij} P_k P_l + \frac{1}{2} g_{ijkl} (\partial P_i / \partial x_j) (\partial P_k / \partial x_l) - \frac{1}{2} \kappa_0 E_i E_i - E_i P_i, \quad (1)$$

in which the repeated indices imply summing over 1, 2 and 3. The first three terms in Eq. (1) represent the Landau-Devonshire free energy, where  $\alpha_i = (T - T_0) / 2\varepsilon_0 C_0$  is the dielectric stiffness,  $\alpha_{ij}$  and  $\alpha_{ijk}$  are higher order dielectric stiffnesses,  $T$  and  $T_0$  denote the temperature and the Curie-Weiss temperature, respectively,  $C_0$  is the Curie constant. The fourth term denotes the elastic energy of the system, in which  $c_{ijkl}$  is the elastic constant. The fifth term is the coupling energy between polarizations and strains, where  $q_{ijkl}$  is the electrostrictive coefficient. The term of  $\frac{1}{2} g_{ijkl} (\partial P_i / \partial x_j) (\partial P_k / \partial x_l)$  is the gradient energy, in which  $g_{ijkl}$  is the gradient coefficient. The gradient energy gives the energy penalty for spatially inhomogeneous polarization. Except for the last two terms, all the other terms in Eq. (1) are the same as those in Refs. [17] and [18]. The last two terms are introduced through Legendre transformation in order to obtain the electrical enthalpy, in which  $\kappa_0$  is the dielectric constant of vacuum. With the electrical enthalpy, the stresses and electric displacements can be derived as  $\sigma_{ij} = \partial h / \partial \varepsilon_{ij}$  and  $D_i = -\partial h / \partial E_i$ .

The temporal evolution of the polarization formation in ferroelectrics can be obtained from the following time-dependent Ginzburg-Landau equation

$$\frac{\partial P_i(\mathbf{x},t)}{\partial t} = -L \frac{\delta F}{\delta P_i(\mathbf{x},t)} \quad (i=1, 2, 3), \quad (2)$$

where  $L$  is the kinetic coefficient,  $F = \int_V h dv$  is the total free energy of the simulated system,

$\delta F / \delta P_i(\mathbf{x},t)$  represents the thermodynamic driving force for the spatial and temporal evolution of the simulated system,  $\mathbf{x}$  denotes the spatial vector,  $\mathbf{x} = (x_1, x_2, x_3)$ , and  $t$  is time.

In addition to Eq. (2), the following mechanical equilibrium equation

$$\frac{\partial}{\partial x_j} \left( \frac{\partial h}{\partial \varepsilon_{ij}} \right) = 0 \quad (3)$$

and Maxwell's (or Gauss') equation

$$\frac{\partial}{\partial x_i} \left( -\frac{\partial h}{\partial E_i} \right) = 0 \quad (4)$$

must be simultaneously satisfied for charge-free and body-force-free ferroelectric materials. A nonlinear multi-field coupling finite element formulation is developed to solve the governing equations (2), (3) and (4). In the space discretization, an eight-node brick element is employed with seven degrees of freedom at each node. The seven degrees of freedom include three displacements, one electrical potential and three polarizations. The detailed derivation of the developed three-dimensional finite element formulation of ferroelectrics will be published somewhere else. Compared with the three-dimensional phase field simulations of ferroelectrics in the literature,<sup>16,19</sup> the present finite-element phase field model does not employ periodic boundary conditions. It is able to simulate ferroelectrics with complex boundary conditions and geometrical shapes, such as FNTs with different mechanical and electrical boundary conditions.

We take  $\text{PbTiO}_3$  FNTs as an example to study how the electrical boundary condition affects the equilibrium polarization distribution. All the materials constants used in the simulation are the same as those of Refs. [20, 21]. In the simulations, we employ 8000 discrete brick elements to model the FNTs with 20 elements in the longitudinal direction (in the  $x_3$  axis direction), 40 elements in the annular direction and 10 elements in the radial direction. The longitudinal length of the simulated FNTs is 6nm, and the inner and outer radii are 4 nm and 8 nm, respectively. The FNTs are assumed to be free-standing, which means that the surfaces of the tubes are mechanically traction free, i.e.  $\sigma_{ij}n_j = 0$ , where  $n_j$  denote the components of the normal unit vector of the surfaces. For the surfaces with open-circuit electrical boundary conditions, the charge density is taken to be zero. It implies the normal component of the electric displacement is zero, i.e.  $D_i n_i = 0$ , on the surfaces. For the surfaces with short-circuit electrical boundary conditions, the electrical potential is taken as zero in the simulation. The free boundary condition of  $\partial P / \partial n = 0$  is used for the polarizations on the surfaces,<sup>22</sup> which means that there is no surface effect on the polarization. We take this boundary condition because there is still a debate on whether the polarizations on surfaces are smaller or larger than those inside the ferroelectrics. The backward Euler scheme is adopted for the time integration in Equation (2). At the beginning of the evolution, a random fluctuation of polarization field is introduced to initiate the polarization evolution process.<sup>16,21</sup> At the end of the evolution, the simulated system reaches a steady state. In the present letter, only the results at the steady state and at room temperature are presented.

Fig.1 (a) shows the three-dimensional polarization vectors in a ferroelectric nanotube with all surfaces are open-circuited. One can find that the polarizations form a vortex structure, in which the vortex axis coincides with the symmetry axis of the nanotube, i.e. the  $x_3$  axis. The contour legend shows different magnitudes of polarizations in different colors.

Fig.1 (b) gives the two-dimensional projection of the three-dimensional polarization vectors in the middle plane of the nanotube with  $x_3 = 3$  nm. The zero point of the  $x_3$  axis is located at the center of the lower surface. The  $x_3$  axis is outward and perpendicular to the  $x_1x_2$  plane. It is found that the polarizations form into closed loops in the annular direction of the nanotube. The polarizations have a head-to-tail arrangement, which greatly reduces the depolarization energy. The polarization components normal to the outer and inner surfaces approach zero. Therefore, there is no polarization-induced charge on the two surfaces. The polarizations between the outer and inner surfaces have no radial components. So there is also no charge generated inside the tubes and the depolarization field in the radial direction is zero. These results are reasonable for an open-circuit electrical boundary condition. Under such a condition, surface charges can not be compensated by external free charges. If the polarization components in the radial direction are not zero, uncompensated charges will exist on the outer and inner surfaces. The uncompensated charges will generate a depolarization field. To reduce the depolarization energy, all the polarizations must be perpendicular to the radial direction of the tube.

It is interesting that the polarizations change their magnitudes in both the radial and the annular directions. Fig.1 (c) gives the magnitude of polarization changes along the annular direction in the middle plane with different radii  $R$  shown in Fig.1 (b). The horizontal axis in Fig.1 (c) is the angular coordinate  $\theta$  shown in Fig.1 (b), which changes from 0 to  $2\pi$ . The fluctuation of the magnitudes of polarizations in Fig.1 (c) is similar to a sine function. Furthermore, the fluctuation on the outer surface with  $R=8$  nm is different from that of the inner surface with  $R=4$  nm. The fluctuations on the two surfaces are “out of phase”, in which one reaches a maximal value while the other takes a minimal value. However, the fluctuation becomes smaller at the middle of the tube wall when  $R=6$  nm, indicated by the solid line with triangles in Fig.1 (c). A pure vortical distribution of polarization without components in the

$x_3$  direction is energetically favorable for the electrostatic interaction, but not for the elastic interaction. To reduce the elastic energy, some polarizations have a component in the  $x_3$  direction. Fig. 1 (d) shows the changes of polarization component  $P_3$  along the annular direction on the outer surface for different heights  $x_3$ . One can find that  $P_3$  changes its sign with different values of  $\theta$ . In the middle plane of the tube, the polarization component  $P_3$  has maximum magnitude. The magnitudes of  $P_3$  gradually decrease from the middle plane to the lower surface of the tube, as shown in Fig. 1 (d).  $P_3$  approaches zero on the lower surface with  $x_3 = 0$ . The vanishing of the normal component  $P_3$  on the lower surface is consistent with the open-circuit boundary condition of  $D_i n_i = 0$ .

In order to investigate the influence of different electrical boundary conditions on the polarization distribution in FNTs, we study two kinds of short-circuit electrical boundary conditions. One is the outer and inner surfaces are short-circuited. Fig.2 (a) shows the three-dimensional polarization vectors on the surfaces of the tube with such a boundary condition. We can find that most of the polarizations are perpendicular to the longitudinal direction. The polarizations do not form a vortex structure along the annular direction any more. Instead, some of the polarizations align along the radial direction of the tube. Fig.2 (b) shows the two-dimensional projection of the three-dimensional polarization vectors in the middle plane of the tube. Under the short-circuit boundary condition, the polarization components normal to the inner and outer surfaces are nonzero, and the surface charges induced by the polarizations in the radial direction are compensated completely by external free charges. So the radial polarization components will not generate a depolarization field. On the other hand, there is still an internal depolarization field induced by inhomogeneous polarizations inside the tube. The charges induced by inhomogeneous polarizations inside the tube can not be compensated by external free charges due to the nonconductive nature of ferroelectrics. In Fig.2 (b), the

polarizations in the red region have the same orientation, while the polarizations in the blue region have another orientation.  $90^\circ$  domain walls are formed in the ferroelectric nanotube. Even though the tube is freestanding, there are internal stresses induced by the spatially inhomogeneous polarizations through the electromechanical coupling. The formation of  $90^\circ$  domain walls is to reduce the total elastic energy in the tube. Although a homogeneous polarization distribution has the minimum depolarization energy, it makes larger elastic energy than the inhomogeneous one in the tube. Therefore the multi-domain structure of the polarizations in Fig. 2 (b) is the result of the competition between the elastic energy and the depolarization energy.

Figure 3 shows the polarization distribution in a ferroelectric nanotube when the upper and lower surfaces are short-circuited. Under such a condition, all the polarizations are aligned along the longitudinal direction. We can find that the polarizations of the FNTs form a single-domain structure without any domain walls. The polarizations are homogeneous in both the longitudinal and the radial directions. This polarization distribution does not induce any elastic energy and depolarization energy in the tube. The charges induced by the polarizations on the upper and lower surfaces are compensated completely by external free charges under the short-circuited electrical boundary condition. The macroscopic averaged polarization is nonzero in the  $x_3$  direction. Therefore, the whole tube exhibits a piezoelectric effect even without poling. This is different from the case in Fig.1, in which there is no piezoelectric effect due to the null macroscopic averaged polarization.

In summary, we predict that the polarization distributions of FNTs are highly dependent on the electrical boundary conditions. Because there is no charge compensation on the surfaces under an open-circuit boundary condition, all the polarization components normal to the surfaces vanish, which makes FNTs form a vortex structure with null macroscopic



polarization. When charge compensations take place at different surfaces, corresponding to different short-circuit boundary conditions, different polarization distributions are found. If full charge compensations take place on the inner and outer surfaces of FNTs, the polarizations are parallel to the upper and lower surfaces and some of them are aligned along the radial direction of the tubes. However, the polarizations form a single-domain structure with all polarizations in the longitudinal direction when full charge compensations take place on the upper and lower surfaces. The results in the present work suggest that the stable polarization distribution in FNTs can be manipulated by different electrical boundary conditions.

## Acknowledgements

JW gratefully acknowledges the Alexander von Humboldt Foundation for awarding a research fellowship to support his stay at Forschungszentrum Karlsruhe.

## References

- <sup>1</sup>W.L. Zhong, Y.G. Wang, P.L. Zhang, and B.D. Qu, Phys. Rev. B **50**,698 (1994).
- <sup>2</sup>I. Ponomareva, L. Bellaiche, and R. Resta, Phys. Rev. Lett. **99**, 227601 (2007).
- <sup>3</sup>C. Ahn, K. Rabe, and J. Triscone, Science **303**, 488 (2004).
- <sup>4</sup>I.I. Naumov, L. Bellaiche, and H. Fu, Nature (London) **432**, 737 (2004).
- <sup>5</sup>S. Prosandeev, I Ponomareva, I Korrev, I. Naumov, and L. Bellaiche, Phys. Rev. Lett. **96**, 237601 (2006).
- <sup>6</sup>J.E. Spanier, A.M. Kolpak, J.J. Urban, L. Grinberg, L. Ouyang, W.S. Yun, A.M. Rappe, and H. Park, Nano Lett. **6**, 735 (2006).
- <sup>7</sup>A. Schilling, R.M. Bowman, G. Catalan, J.F. Scott, and J.M. Gregg, Nano Lett. **7**, 3787 (2007).

- <sup>8</sup>J. Junquera, and P. Ghosez, *Nature (London)* **422**, 506 (2003).
- <sup>9</sup>S.K. Streiffer, J.A. Eastman, D.D. Fong, C. Thompson, A. Munkholm, M.V.R. Murty, O. Auciello, G.R. Bai, and G.B. Stephenson, *Phys. Rev. Lett.* **89** (2002).
- <sup>10</sup>F. Morrison et al., *Rev. Adv. Mater. Sci.* **4**, 114 (2003).
- <sup>11</sup>Y. Luo, I. Szafraniak, N.D. Zakharov, V. Nagarajan, M. Steinhart, R.B. Wehrspohn, J.H. Wendorff, R. Ramesh, and M. Alexe, *Appl. Phys. Lett.* **83**, 440 (2003).
- <sup>12</sup>Y. Yang, X.H. Wang, C.F. Zhong, C.K. Sun, and L.T. Li, *Appl. Phys. Lett.* **92** (2008).
- <sup>13</sup>J. Kim, Y. Choi, and S. Bu, *Ferroelectrics* **356**, 528 (2007).
- <sup>14</sup>J. Scott, *Nat. Mater.* **4**, 13 (2005).
- <sup>15</sup>J. Wang, M. Kamlah, T.Y. Zhang, Y.L. Li and L.Q. Chen, *Appl. Phys. Lett.* **92**, 162905 (2008).
- <sup>16</sup>Y.L. Li, S.Y. Hu, Z.K. Liu, and L.Q. Chen, *Appl. Phys. Lett.* **78**, 3878 (2001).
- <sup>17</sup>W. Cao, and L. Cross, *Phys. Rev. B* **44**, 5 (1991).
- <sup>18</sup>S. Nambu, and D Sagala, *Phys. Rev. B* **50**, 5838 (1994).
- <sup>19</sup>J. Slutsker, A. Artemev, and A. Roytburd, *Phys. Rev. Lett.* **100**, 087602 (2008).
- <sup>20</sup>N. Pertsev, A. Zembilgotov, and A. Tagantsev, *Phys. Rev. Lett.* **80**, 1988 (1998).
- <sup>21</sup>J. Wang, S.Q. Shi, L.Q. Chen, Y.L. Li, and T.Y. Zhang, *Acta. Mater.* **52**, 749 (2004).
- <sup>22</sup>Vendik, and S. Zubko, *J. Appl. Phys.* **88**, 5343 (2000).

### Figure captions

Fig.1 Polarization distribution in a ferroelectric nanotube when all surfaces are open-circuited.

(a) Three-dimensional polarization vectors in the ferroelectric nanotube; (b) Two-dimensional projection of the three-dimensional polarization vectors in the middle plane when  $x_3 = 3 \text{ nm}$ ; (c) Magnitudes of polarizations change along the annular direction of the tube in the middle plane with different radii  $R$ ; (d) Polarization components  $P_3$  change along the annular direction on the outer surface of the tube with different heights  $x_3$ .

Fig.2 Polarization distribution in a ferroelectric nanotube when the inner and outer surfaces are short-circuited. (a) Three-dimensional polarization vectors in the ferroelectric nanotube; (b) Two-dimensional projection of the three-dimensional polarization vectors in the middle plane of the tube when  $x_3 = 3 \text{ nm}$ .

Fig.3 Polarization distribution in a ferroelectric nanotube when the upper and lower surfaces are short-circuited. The polarizations are homogeneous and parallel to the  $x_3$  axis. Only half of the tube is shown here, the hidden part has the same polarization distribution.

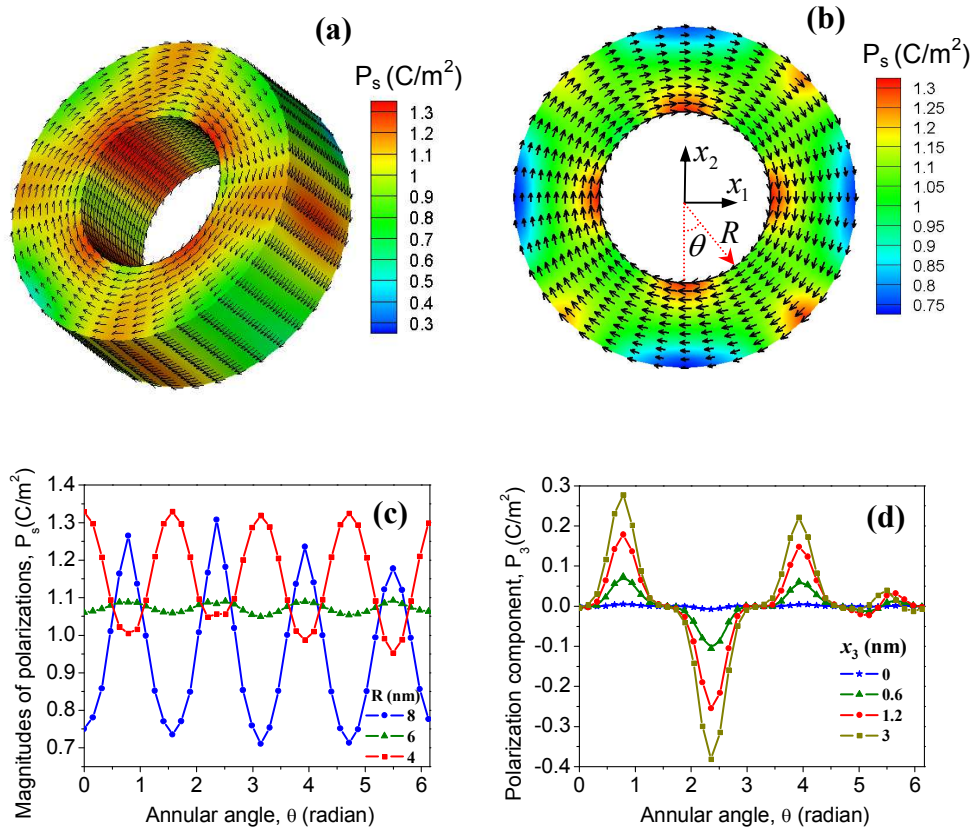


Fig.1 Polarization distribution in a ferroelectric nanotube when all surfaces are open-circuited. (a) Three-dimensional polarization vectors in the ferroelectric nanotube; (b) Two-dimensional projection of the three-dimensional polarization vectors in the middle plane of the tube when  $x_3 = 3 \text{ nm}$ ; (c) Magnitudes of polarizations change along the annular direction of the tube in the middle plane with different radii  $R$ ; (d) Polarization components  $P_3$  change along the annular direction on the outer surface of the tube with different heights  $x_3$ .

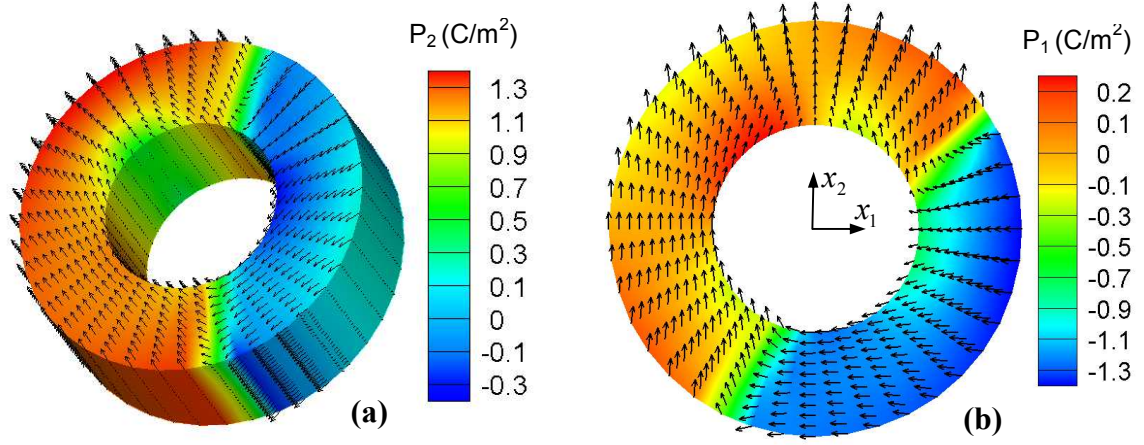


Fig.2 Polarization distribution in a ferroelectric nanotube when the inner and outer surfaces are short-circuited. (a) Three-dimensional polarization vectors in the ferroelectric nanotube; (b) Two-dimensional projection of the three-dimensional polarization vectors in the middle plane of the tube when  $x_3 = 3 \text{ nm}$ .

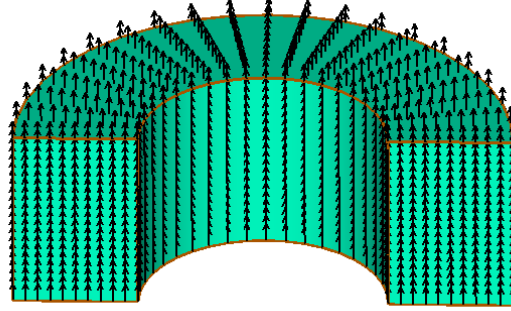


Fig.3 Polarization distribution in a ferroelectric nanotube when the upper and lower surfaces are short-circuited. The polarizations are homogeneous and parallel to the  $x_3$  axis. Only half of the tube is shown here, the hidden part has the same polarization distribution.